A direct spinal cord–computer interface enables the control of the paralysed hand in spinal cord injury

Daniela Souza Oliveira,[1,†] Matthias Ponfick,[2] Dominik I. Braun,[1] Marius Osswald,[1] Marek Sierotowicz,[1,5] Satyaki Chatterjee,[1] Douglas Weber,[3,4] Bjoern Eskofier,[1,6] Claudio Castellini,[1,5] Dario Farina,[7] Thomas Mehari Kinfe[1,8,‡] and Alessandro Del Vecchio[1,†,‡]

†,‡**These authors contributed equally to this work.**

Abstract

The paralysis of the muscles controlling the hand dramatically limits the quality of life of individuals living with spinal cord injury (SCI). Here, with a non-invasive neural interface, we demonstrate that eight motor complete SCI individuals (C5-C6) are still able to task-modulate in real-time the activity of populations of spinal motor neurons with residual neural pathways.

In all SCI participants tested, we identified groups of motor units under voluntary control that encoded various hand movements. The motor unit discharges were mapped into more than 10 degrees of freedom, ranging from grasping to individual hand-digit flexion and extension. We then mapped the neural dynamics into a real-time controlled virtual hand. The SCI participants were able to match the cue hand posture by proportionally controlling four degrees of freedom (opening and closing the hand and index flexion/extension).

These results demonstrate that wearable muscle sensors provide access to spared motor neurons that are fully under voluntary control in complete cervical SCI individuals. This non-invasive neural interface allows the investigation of motor neuron changes after the injury and has the potential to promote movement restoration when integrated with assistive devices.

Author affiliations:

1 Department Artificial Intelligence in Biomedical Engineering, Friedrich-Alexander-Universität Erlangen-Nürnberg, 91052 Erlangen, Germany

2 Querschnittzentrum Rummelsberg, Krankenhaus Rummelsberg GmbH, 90592 Schwarzenbruck, Germany

3 Department of Mechanical Engineering, Carnegie Mellon University, Pittsburgh, PA 15213, USA

4 Neuroscience Institute, Carnegie Mellon University, Pittsburgh, PA 15213, USA

5 Institute of Robotics and Mechatronics, German Aerospace Center (DLR), 82234 Oberpfaffenhofen, Germany

6 Translational Digital Health Group, Institute of AI for Health, Helmholtz Zentrum München - German Research Center for Environmental Health, 85764 Neuherberg, Germany

7 Department of Bioengineering, Imperial College London, London, SW7 2AZ, UK

8 Division of Functional Neurosurgery and Stereotaxy, Friedrich-Alexander-Universität Erlangen-Nürnberg, 91054 Erlangen, Germany

Correspondence to: Alessandro Del Vecchio

Department Artificial Intelligence in Biomedical Engineering, Faculty of Engineering

Friedrich-Alexander-Universität Erlangen-Nürnberg

Henkestraße 91, 91052 Erlangen, Germany

E-mail: alessandro.del.vecchio@fau.de

Correspondence may also be addressed to: Daniela Souza de Oliveira

E-mail: daniela.s.oliveira@fau.de

Keywords: spinal cord injury; motor neuron; motor unit; high density surface electromyography; neural interface

Abbreviations: HDsEMG = High-density surface electromyography; PPS = Pulses per Second; SCI = Spinal Cord Injury

Introduction

Impaired hand function is arguably one of the most severe motor deficits in subjects with spinal cord injury (SCI), especially when bilateral[1]. There are currently no effective treatments for regaining hand control after muscle paralysis. Hand surgery is established, although not possible in every case, and with several challenges, such as reconstruction of intrinsic hand function and requiring precise diagnostics and planning[2]. Restoration of hand function has so far been achieved by neural interfaces recording the activity of the motor cortex[3], either through closed-loop electrical stimulation of the muscle[4] or by controlling external devices[5]. However, besides the relatively poor control, invasive cortical implants are also an option limited to a small proportion of patients because of the surgical risks and long-term stability of the implant. Other neural interfaces involve the delivery of electrical stimulations in the spinal cord that indirectly target the activity of the alpha motor neurons[6].

The neural information most directly associated with behavior is the activity of spinal alpha motor neurons, representing the final neural code of movement. The activity of spinal motor neurons generates movement through a simple transformation (the dynamics of the twitch forces of the muscle units), and therefore, movement intent can be decoded directly. Almost all SCIs are due to contusions of the spinal cord, which could leave some spared connections above and below the level of the injury[7]. While this spared neural activity is insufficient to drive muscles to generate detectable forces, it can be used to infer motor intent and, therefore, to decode movements. Accordingly, as a case study, we have recently reported in a single motor-complete SCI (C5-C6) individual the presence of a significant number of task-modulated motor units encoding the flexion and extension of individual fingers through a wearable, non-invasive neural interface[8]. That case study was a proof of concept in a single patient, and it was limited to offline analysis without any demonstration of patient-in-the-loop control. Here, we support previous evidence of voluntarily controlled spinal motor neurons in eight SCI individuals (injury levels ranging from C5 to C6)[7–10]. Through the decomposition of the high-density surface electromyogram (HDsEMG)[11–13], we identified active motor neurons in all tested patients (Fig. 1). These motor neurons encoded the movements of the

paralyzed hand during synergistic and individual digit movements. The discharge patterns of the motor neurons were similar to those observed in non-injured young adults. The motor neurons followed precise recruitment and discharge rate patterns that closely matched the movements of the virtual hand. This study shows that even many years after chronic SCI, there are still spared motor neurons that receive functional inputs modulated by voluntary intent.

Materials and methods

Participants

Eight participants with SCI were recruited for this study (seven individuals with chronic motor complete SCI and one with motor incomplete SCI – Fig. 2 and Table 1). The inclusion criteria were: (1) injury level C4-C6, (2) age between 18 and 60 years old, and (3) absence of voluntary movement of one hand or both hands. Participants S6 and S7 have functional left hands.

In Table 1, we reported information from standard clinical examinations of the SCI group regarding clinical classification of injury according to the American Spinal Injury Association (ASIA) impairment scale; spasticity assessment through the modified Ashworth scale and testing of upper limb stretch reflexes (biceps, triceps, and brachioradialis tendon reflexes). In Supplementary Figure 1, we reported T2-weighted MRI images from the SCI group's medical history to depict the location and diversity of the injuries.

Additionally, we recruited 12 healthy, uninjured subjects (control group, age 27.1 ± 3.4 years, two females) for comparison.

All participants gave their written informed consent to take part in the study. The study was conducted in agreement with the Declaration of Helsinki and was approved by the Friedrich-Alexander-Universität Ethics Committee (applications 22-138-Bm and 21-150-B).

Study overview and experimental protocol

This study was conducted in two sessions. In the first session, we asked the participants to attempt the movements displayed by videos of a virtual hand. At the same time, we recorded HDsEMG signals from their forearm muscles. For the second session, six subjects from the SCI group returned after 3-5 months of the first session (S1-S4, S6, and S8), in which a

regression model (based on global EMG) and/or an online decomposition method was used to decode movement intention, according to their HDsEMG signals.

In the first session, according to their forearm circumference, we placed 256 or 320 HDsEMG electrodes on the forearm of the participants' dominant hand (S7 was paralyzed only on the non-dominant hand). The electrodes covered the forearm muscles and the wrist. We chose this placement to maximize the number of electrodes and, thus, improve the accuracy of HDsEMG decomposition since we can also detect far-field electrical potentials at the wrist [14]. For the SCI group, after placing the electrodes, we asked the subjects to stay in a comfortable position with their arms (Fig. 1A, Fig. 5B, and 5F). For the control group, the participants were standing with their dominant elbows flexed (this setup was previously described [15]). To both groups, we showed the same videos of a virtual hand performing different tasks on a computer monitor and instructed the participants to attempt the movements accordingly. The tasks lasted 42s each and included flexion and extension of the individual digits at two speeds (0.5Hz and 1.5Hz), grasp, two-finger pinch, three-finger pinch, and wrist flexion and extension (0.5Hz). Two trials were performed for each movement (only for the SCI group). We only analyzed data from slow (0.5Hz) movements as the subjects reported difficulty performing the fast ones.

In the second session, we tested a real-time EMG decomposition approach (brief offline decomposition followed by online decomposition, Fig. 5C-D). We used 128 HDsEMG electrodes to assess if the subjects would be able to follow a digital trajectory with their motor units smoothed cumulative discharge rate. First, during the offline decomposition, we recorded HDsEMG data while the participants attempted a maximum flexion of the digits (10s per task). This data was decomposed as described in the 'Online decomposition' section (Supplementary material), and we stored the decomposition results for the online task.

Subsequently, in the online decomposition step, we instructed the subjects to follow a periodic rectangular waveform trajectory shown on a monitor, with 10s period (5s of rest in between), for 60-120s. The trajectories have two different activation levels, 20% and 30% of maximum neural activation, i.e., of the maximum discharge rate obtained during the brief offline decomposition step. These activation values should not be confused with the maximal voluntary force obtained in healthy individuals. It could be impossible for a person to modulate the discharge rate of a specific motor unit up to its maximum for a prolonged time. This is because of the nonlinear behavior of motor units due to the spike-frequency adaptation and the discharge rate modulation due to intrinsic motor neuron properties [16–18].

The subjects attempted flexion and extension of the same digits for two consecutive periods as performed in the offline decomposition with 20% maximum neural activation. The motor unit firings detected with this method (smoothed motor unit firings) were shown as feedback to the subjects. Lastly, we also tested if the participants could modulate their discharge rate and progressively recruit motor units by increasing the height of the ramp to 30% maximum neural activation and alternating between the two activation levels (Supplementary Video 1).

Also, an EMG-to-activation regression model was generated in the second session using the same electrode configuration as in the first visit. During this session, we asked the subjects to indicate which tasks from the first session they could perform with the least effort. These tasks were, therefore, selected to build the model. For that, the subjects were asked to attempt the maximal/full flexion of these tasks (e.g., the selected task was index movement; thus, they had to perform an index maximal flexion to build the model). These EMG signals were acquired and associated to the synthetic ground truth representing maximal activation for the relevant degrees of freedom. After that, the participants attempted the flexion and extension of the digits according to their chosen tasks. The predicted activation was shown in real-time through a virtual hand interface ('predicted hand', Fig. 5F, Supplementary Video 2). We used a virtual hand showing a predefined movement (referred here as 'control hand', Fig. 5F, H-I) to help the subjects to perform the movements and for further analysis.

For complete information on the recordings and data analysis, see Supplementary Material.

Results

To assess the extent of spared motor unit activity in SCI participants, we analyzed the number of identified motor units, the reconstructed HDsEMG signals (motor unit action potential shapes convolved with motor unit firings), discharge rate, and coherence area values. We compared these measures to those of the control group. Additionally, we evaluated the outcomes of the real-time decomposition and virtual hand control.

Figure 1 shows an overview of the offline experiments. We asked the subjects to match the visual cue displayed through a virtual hand (hand opening and closing, two and three-finger pinch, and flexion and extension of individual digits at 0.5Hz movement velocity). Figure 1A shows the experimental setup, with 320 electrodes placed on the proximal and distal forearm muscles and tendons (wrist). Figure 1B-C illustrates six EMG channels and a motor unit

waveform superimposed on a heatmap based on the root mean square activity. In all tested patients, we observed clear motor unit action potentials with high signal-to-noise ratio (>26dB[19]). We then looked at how these motor units were controlled by studying the association between motor unit activation times (Fig. 1D) and the attempted movement by looking at the trajectories of the digit tip of the virtual hand (grey curve in Fig. 1D). The raster plot in Fig. 1D shows a clear grouping of motor units encoding flexion and extension movements during a grasping task. As in our previous experiment[8], we used a factorization method to retrieve the motor dimension (flexion and extension of the motor units, Fig. 1E-F). For all tested individuals, we consistently identified some motor neurons that were controlling the flexion and extension movements (Supplementary Figs. 2-9). From the power spectrum of the neural modules (Fig. 1G), we found a peak at the movement frequency 0.5Hz and lower frequencies. Figure 1H-I shows the coherence values across all tasks of subject 6 (mean) and the coherence peak for the delta (1 - 5Hz), alpha (6 - 12Hz), beta (15 - 30Hz), and gamma (31 -80Hz) bandwidths.

Table 1 and Supplementary Figure 1 show a summary of all subjects and tasks, including a description of the SCI through T2-weighted MRI. Details regarding the sensory level of the injury, stretch reflexes, and spasticity are also presented in Table 1. We provide a comparison between raw EMG signals of SCI and control groups in Fig.2A and Fig.6. For all the tasks (Fig. 2C, Table 1), we identified a specific subpopulation of motor units that encoded that particular movement, with an average of 9.8 ± 6.0 motor units per task across all SCI subjects. We also identified unique motor units for each task (Table 1). In Figure 2B, we show the number of motor units across all tasks for each subject for SCI and control groups. Across tasks of the same subject, the variability in the number of motor units is low, with a standard deviation (SD) between 1-2 motor units for all subjects except S6, where we have SD = 4. For the control group, we observed an average of 8.0 ± 4.1 motor units per task across all participants. The groups present similar median values (Fig. 2D), with no significant difference regarding the number of decomposed motor units (generalized linear mixed-effects: $\beta = 0.007$, $t(144) = 1.10$, p-value = 0.27). This information shows that SCI subjects still present a relatively high number of motor units.

Due to the similar number of identified motor units between the groups, we conducted an additional analysis to determine if the HDsEMG data detected most of the active motor units in the SCI group. It is important to note that the number of detected motor units is not directly related to the total number of motor units, as many methodological factors influence it (see

[20,21] for more information). First, we extracted the motor unit action potential shapes from the decomposed HDsEMG signals and convolved these shapes with the motor unit firings to reconstruct the EMG signal. We then calculated the root mean square error (RMSE) between the original and reconstructed EMG signals to measure the residual EMG activity (see Supplementary Methods). This value serves as an index of the undecomposed motor units and the total number of active motor units for a given task. Interestingly, as shown in Fig. 2E-F, we found significantly lower RMSE values in SCI (20.3 ± 16.7μV) in comparison to the control (41.0 ± 18.8 μV) (β = -33.7, t(144) = -4.5, p-value = 1.6e-5). These lower values indicate that we are decomposing a higher proportion of motor units in SCI and that there are fewer active motor units for a specific task.

In Figures 3A-B, we present the average discharge rate in pulses per second (pps) calculated across tasks and subjects. We can observe that the variation in discharge rate is subject-specific (Fig. 3A), with S1, S2, and S3 presenting higher median discharge rates. Comparing the data across subjects of both groups (average discharge rate of SCI = 11 ± 3.2 pps and control = 12.8 ± 2.1 pps per task across all subjects), we can identify S4 to S7 with the lower discharge rates, and S2, S3, and S8 with similar values to the control group. Overall, in Figure 3C, we observed no significant difference between the groups (β = -0.002, t(144) = -1.64, p-value = 0.10).

In Figure 4, we show the average coherence across all subjects and tasks and the area of each frequency bandwidth across subjects. For the delta band, the median area values did not differ across subjects apart from S1 and S6 (delta) with higher values. We found that S1 and S6 are significantly different from S3, S4, and S7 (Kruskal–Wallis's test: H = 40.8, df =7, p-value = 8.7e-7). For the alpha band, only S1 presented a higher median, being significantly different from S2, S4, S6, and S7 (H = 25.2, df =7, p-value = 0.0007). For beta and gamma bands, subjects S1, S3, and S5 presented higher coherence areas in comparison to the other subjects, the distributions from these subjects are significantly higher than S2 (beta band, H = 27.9, df =7, p-value = 0.0002). For gamma, we found S3 with the highest median, significantly different from S2, S4, S6, and S7, also S1 significantly different from S4 (H = 35.4, df =7, p-value =9.5e-6). When comparing it between groups, only beta and gamma bands are significantly higher in the SCI group – and this is only when we consider the tasks as a fixed effect in our generalized linear mixed-effects model (beta band: β = 2.14, t(151) = 2.38, p-value = 0.018; gamma band: β = 0.73, t(151) = 2.75, p-value = 0.007).

Overall, because of the number of motor units detected, we could identify unique units virtually in all recorded tasks (> 2 motor units/task, except for S3 – Table 1), which can allow an accurate and precise classification for all these motor dimensions. Therefore, after years of cervical SCI leading to motor complete paralysis (ranging from 5.0 to 24.2 years, Table 1), these subjects still had spared connections from the motor cortex, impinging the activity of spinal motor neurons. This is evidenced by the fact that some motor units showed high voluntary modulation that matched with the kinematics of the virtual hand videos (Fig. 5A). Figure 5A shows all the identified motor units for all tasks of one individual. These previous results are based on the number of motor dimensions from the offline decomposition of the HDsEMG.

In a second experiment, collected on average 3-5 months after the first session, we tested six subjects again (S1-S4, S6, and S8) with a similar experimental procedure but tuned for real-time control. We asked the subjects to proportionally control a moving cursor on a screen based on the real-time decoding of the discharge timings of motor neurons (Fig. 5C-D). Moreover, these individuals also controlled a virtual hand (Fig. 5F-I, Supplementary Video 2), demonstrating full voluntary control of the decoded neural activity.

We developed a real-time mapping of the discharge timings of motor neurons so that the patients could control a cursor on the screen with the motor unit discharge activity and a virtual hand with the HDsEMG signals (Fig. 5, Supplementary Video 1). After a few seconds of training (Fig. 5D), the subjects were able to control the motor unit firing patterns and progressive recruitment of motor units at different target forces and with high accuracies, i.e., high cross-correlation values between the requested trajectory and the smoothed cumulative motor unit discharge rate (Fig. 5C-D). In this experiment, we also used a supervised machine-learning algorithm to control a virtual hand (Fig. 5F-I, Supplementary Video 2).

Supplementary Video 1 shows a subject controlling the activity of groups of motor units in real-time, modulating the recruitment and discharge rate to proportionally match two different target levels of activation. The motor neuron discharge times were summed and normalized in real time to the number of active neurons so that the patients could modulate a moving object (yellow cursor, Fig. 5C-D) by increasing/decreasing the discharge rates. Figure 5C shows the proportional control of two target levels mediated by both the concurrent recruitment of additional units (grey raster plot) and higher discharge rates. Figure 5D shows a complete recording set that lasted 120 seconds. Note that just after 50 seconds of training, the subject was able to move the cursor on relatively high levels of normalized

motor unit activity. The scaling of the motor unit activity is based on an equation that considers the maximal motor unit discharge activity and the highest number of motor units identified during an offline calibration trial that lasted 10 seconds for each trained task.

We then trained the subjects to move a virtual hand that was displayed on a monitor and to match the movement of a control hand (Fig. 5F-I, Supplementary Video 2). After this training, the subjects could proportionally and repeatedly open and close the hand, when compared to the control hand instructions (Fig. 5I, Supplementary Video 2). Most of the participants were able to proportionally flex and extend the index finger (two degrees of freedom) and open and close the hand (two degrees of freedom). Figure 5F shows the subject's view: the monitor displayed two hands, a control hand (white color) and a second hand controlled by a regression-based machine learning algorithm. Four out of six subjects (Fig. 5G) were able to control four degrees of freedom consisting of proportional control of index flexion and extension and hand opening and closing (Fig. 5H-I, Video 2).

Discussion

The results above confirm previous evidence of voluntarily controlled spinal motor neurons in subjects with SCI (motor complete ranging from C5 to C6) that have been paralyzed for decades[7–10]. We observed the presence of active modulation of motor neuron activity in all tested patients, with motor units associated with flexion or extension of movements of the paralyzed hand digits. This association is evidenced by the real-time proportional control of the spinal motor neurons, complex movements of the virtual hand, and the factorization analysis results, in which two modules (flexion and extension) explained most of the variance for the movements of each subject. Although the power spectrum of the extracted neural modules shows a peak at the movement frequency, these modules seem to be relatively out of phase and/or delayed for some tasks. These offline results agree with our previous single-case study[8].

Although there is variability in the number of identified motor units across subjects, this number is statistically comparable to the number of motor units found in the control group. For several reasons, we hypothesized that more motor units would be detected for the SCI group. First, the decomposition of HDsEMG signals relies on the total number of active motor units, so the higher this number, the more complex it is for the algorithm to separate the individual motor units[20,21] (for example, in healthy individuals, we detect more motor

units at 10% of maximal force than at 50%, due to a higher superimposition of higher, larger-threshold motor units). Second, the algorithm works best when there are minimal muscle movements (due to the gearing of the muscle) below the recording electrodes. In the SCI group, due to paralysis, this condition is guaranteed as there is no visible movement or force during the attempted hand movements. Moreover, because of the spinal lesion, the number of motor units that the SCI individuals can voluntarily recruit is low, leading to low background noise on the EMG. In contrast, the control group is likely to have a higher number of motor units that are recruited. Consequently, from a computational perspective, this would allow better detection of motor units by decomposition algorithms. Although we found a high number of motor units for two subjects (S1 and S6, Table 1) with different characteristics (e.g., age, injury), this was not observed for the rest of the SCI group. This might indicate a lower number of active motor units for the other subjects of this group.

We further conducted an analysis comparing the filtered-original EMG and the reconstructed EMG. By reconstructing the EMG using the decomposed motor units, we could estimate the residual EMG activity, which is related to the motor units that were not decomposed. As anticipated, we found that the SCI subjects showed smaller RMSE values than the control group, suggesting that we likely decomposed the majority of the spared motor units present in the EMG signal.

The discharge rate is highly variable across subjects and tasks, with three participants presenting a higher median discharge rate than the others. The discharge rate across tasks varies from 7-21 pps, and it is comparable with our control group. Even though the absence of visible movement, the motor unit discharges are still within the range for voluntary contractions in non-injured healthy young adults [22]. This finding supports the idea that the discharge rate can be applied as user feedback for controlling the proposed interface.

The coherence values indicate that the motor neurons share common synaptic inputs, and therefore, a few active motor neurons can be representative of a large pool of motor neurons and used for decoding. In the SCI group, we did not observe a clear pattern of coherence area across subjects. Some subjects present concurrently higher beta and gamma coherence than others, influencing the comparison across groups, with beta and gamma being higher than in the control group. Previous literature describes a possible decrease in beta, with reduced corticospinal input after SCI, and an increase in gamma coherence as compensatory[23–26]. However, a few potential limitations should be considered. First, our results should be validated by a larger number of participants. Second, the coherence values include both

intramuscular and intermuscular coherence. Therefore, we are not able to distinguish the motor units from specific motor pools**.** Last, we could not perform motor-evoked potential measurements, and further electrophysiological measurements are necessary to assess the function and integrity of corticospinal pathways.

Despite that, beta coherence is significantly associated with cortical control since peripheral beta coherence has been shown to be correlated with electroencephalography (EEG) cortical beta during voluntary movements[27]. In addition, beta activity has also been shown to be volitionally modulated through neurofeedback, which could be applied in training SCI participants[27]. Future experiments, including motor-evoked potentials[28,29] and other experimental paradigms[30,31] could highlight potential differences in descending pathways from the cortex and brainstem in controlling flexors and extensor motor units.

Additionally, we did not observe any specific relations between the behavior of the active motor units (discharge rate, coherence) and the spasticity level, stretch reflex, and sensory level of the injury obtained from clinical examinations. However, this may be attributed to the variability between subjects and the relatively low number of tested patients (n=8). Since we have no more information on the residual sensory and motor pathways, we are limited to understand which characteristics could be related to this residual voluntary control. This should be examined in future studies.

Regarding the number of motor units for each task, overall, we found at least 2 unique motor units per task, except for S3 (Figure 2, Table 1). The unique motor units are defined as motor units that are recruited only during one attempted movement. Once they are activated, we can be sure that the SCI individual is attempting a specific movement. This finding confirms that the motion intent of individuals with SCI can be decoded through our non-invasive interface. According to our real-time tests and previous work[8], at least 1-2 unique motor units per task are necessary for our detection approach and to be able to decode more complex movements. The number of detected motor units for each task is crucial for the neural interface performance. The number of unique motor units influences the classification of specific motor dimensions (e.g., index vs middle finger tasks) and the stability of the control over time. It is important to note that a decreased error in the control has been observed with more decoded units due to the averaging effects caused by a large number of motor units firing synchronously[32].

Finally, given the number of specific task-modulated motor units found, we developed a real-time mapping of the discharge timings of motoneurons so that the patients could control a cursor on a monitor and a virtual hand, through an EMG-to-activation regression model. The tested patients performed both cursor and virtual hand tasks accurately and proportionally, demonstrating full voluntary control of the decoded neural activity with the ability to modulate the motor units' discharge rate. Interestingly, all the patients could proportionally control the cursor to 20% and 30% of maximal activation. For the control of a prosthetic device, the proportional control of a motor unit firing activity from 1% to 30% would be sufficient to obtain a large output of forces that could be controlled with, for example, a brushless motor. Therefore, this relatively low range should not indicate a problem in the method but rather a strength of the approach.

Regarding the virtual hand control, this approach is based on a linear regressor model, including an adaptive filter[40], that learns and maps combinations of EMG activity into the movement of the virtual hand. To build the regressor model, we defined artificial labels associated with the movements. Therefore, independent of the capabilities of the user, there is a possible linear superposition of the output labels used during the training of the machine learning model due to the similarity between EMG patterns related to the different movements. Consequently, some accessory movements of the virtual hand might occur. For this reason, the virtual hand control performance was evaluated simply by task completion[33,34].

Moreover, it is important to note that no extensive training was required from the subjects when performing the tasks. Each experiment across all patients did not last more than 3 hours, and we used most of this time to place the electrodes and explain the tasks. Although we did not measure the time it took for the subjects to control the virtual hand and 2D cursor control, we estimate less than 30 minutes, even for the individuals with the highest level of wrist and hand paralysis. This time can be further improved once the subjects are trained with the tasks. A critical aspect of neural interfaces is the training time and intuitive use. The fact that the subjects learned the tasks in a short training time and were not under fatigue conditions demonstrates the feasibility of the presented approach.

Our results indicate that motor- and sensory-complete SCI individuals maintain relevant neural activity as the output of the spinal cord circuits below the lesion and that they can accurately control this activity to regain hand function. Wearable muscle sensors are accessible, non-invasive, and have the potential to enhance the neural control of assistive

devices and increase the use of these devices. Therefore, this technology may compete in terms of clinical viability and efficacy with current invasive brain or spine implants for restoring hand function in complete SCI patients. While we cannot directly compare these approaches and further tests are needed, our results are similar in task achievement and performance for tasks such as grasping and other hand movements without requiring any surgery and complex models [35–37]. Previous surveys show that a considerable number of tetraplegic and paraplegic patients are reluctant to have cortical implants[3,38,39]. Therefore, we argue that the proposed non-invasive approach might have the potential to be a clinically superior solution for the purpose of hand function restoration in SCI compared to the current invasive brain and spinal neural interfaces.

One important constraint of our approach is that it is inherently linked to spared motor unit activity. Although we found spared motor units in all SCI individuals that were classified as motor complete, this technology may not be effective for subjects with higher levels of complete lesions (C1-C2) and muscles far from the level of the injury. A second constraint is that we calibrate our real-time session in an offline decomposition step by decoding the activity during a predefined task. This implies that the online decomposition is limited by the number of motor units recruited during this first step. Therefore, it is possible that motor units recruited during real-time tasks cannot be detected by our algorithms. This could be further improved by implementing algorithms that work in parallel with the real-time feedback of motor unit data to the patients. Importantly, for the classification of the different hand digit movements, our method is inherently bound to the number of unique motor units that can be found in a task. Furthermore, spasticity could also affect the efficiency of our approach. We observed that some motor units persist in firing even when the voluntary intent stops, and this should also be considered for the development of future algorithms.

Limitations

The current study focuses on HDsEMG measurements, motor unit behavior, and real-time control of motor unit activity. Therefore, this limits the investigation of the mechanisms underlying the residual voluntary activity found in SCI subjects. As spinal motor neurons execute the final motor commands, we have limited information on the spinal and supraspinal inputs that determine the volitional recruitment and modulation of motor unit firings in SCI. Additional electrophysiological and clinical tests, such as stimulation of the brain and spinal cord, might help infer some of the cortical and spinal pathways involved. Consequently, with

the current dataset, we cannot hypothesize about the origins of the synaptic inputs impinging on spinal motor neurons. Future tests should include further medical examinations concurrent with electrophysiological testing at the central and peripheral levels and evoked electrical and magnetic stimulation measurements.

Conclusion

In summary, our results confirm that SCI subjects can voluntarily control residual motor neuron activity. This activity provides enough information to decode movement intent of fine hand tasks. We demonstrated that the presented non-invasive technology could provide intuitive and effective control of the paralyzed hand, even many years after the injury. Our findings could be helpful in the investigation of movement control and recovery mechanisms after SCI through the tracking of the same motor unit across interventions. Therefore, this neural interface has a direct clinical translation for home and hospital use to restore and monitor the spared connections after traumatic SCI. Further work will focus on improving the online control based on motor unit activity related to the different movements and integration with assistive technology, such as exoskeletons and prosthetics.

Data availability

The data that support the findings of this study are available from the corresponding author, upon reasonable request.

Acknowledgements

We would like to thank all participants of this study, especially the ones from the SCI group whose efforts made this study possible.

Funding

This work was supported by the European Research Council (ERC) Starting Grant project GRASPAGAIN under grant 101118089 (ADV); the German Ministry for Education and

Research (BMBF) through the project MYOREHAB under Grant 01DN2300 (ADV); Bavarian State Ministry of Economic Affairs and Media, Energy and Technology through the project NeurOne under grant LSM-2303-0003 (ADV) and the d.hip (Digital Health Innovation Platform), a cooperation between Siemens Healthineers, Medical Valley, University Hospital Erlangen, and Friedrich-Alexander University (ADV and DSO). DF is funded by the European Research Council (ERC) under the Synergy Grant Natural BionicS (810346) and the EPSRC Transformative Healthcare for 2050 project NISNEM Technology (EP/T020970/1).

Competing interests

The authors report no competing interests.

Supplementary material

Supplementary material is available at *Brain* online.

References

1. Snoek GJ, Ijzerman MJ, Hermens HJ, Maxwell D, Biering-Sorensen F. Survey of the needs of patients with spinal cord injury: Impact and priority for improvement in hand function in tetraplegics. *Spinal Cord*. 2004;42(9):526-532. doi:10.1038/sj.sc.3101638

2. Fridén J, House J, Keith M, Schibli S, van Zyl N. Improving hand function after spinal cord injury. *J Hand Surg Eur Vol*. 2022;47(1):105-116. doi:10.1177/17531934211027460

3. Collinger JL, Boninger ML, Bruns TM, Curley K, Wang W, Weber DJ. Functional priorities, assistive technology, and brain-computer interfaces after spinal cord injury. *J Rehabil Res Dev*. 2013;50(2):145. doi:10.1682/JRRD.2011.11.0213

4. Bouton CE, Shaikhouni A, Annetta N V., et al. Restoring cortical control of functional movement in a human with quadriplegia. *Nature*. 2016;533(7602):247-250. doi:10.1038/nature17435

5. Benabid AL, Costecalde T, Eliseyev A, et al. An exoskeleton controlled by an epidural wireless brain–machine interface in a tetraplegic patient: a proof-of-concept demonstration. *Lancet Neurol*. 2019;18(12):1112-1122. doi:10.1016/S1474-4422(19)30321-7

6. Barra B, Conti S, Perich MG, et al. Epidural electrical stimulation of the cervical dorsal roots restores voluntary upper limb control in paralyzed monkeys. *Nat Neurosci*. 2022;25(JulY). doi:10.1038/s41593-022-01106-5

7. Sherwood AM, Dimitrijevic MR, Barry McKay W. Evidence of subclinical brain influence in clinically complete spinal cord injury: discomplete SCI. *J Neurol Sci*. 1992;110(1-2):90-98. doi:10.1016/0022-510X(92)90014-C

8. Ting JE, Del Vecchio A, Sarma D, et al. Sensing and decoding the neural drive to paralyzed muscles during attempted movements of a person with tetraplegia using a sleeve array. *J Neurophysiol*. 2021;127(1):2104-2118. doi:10.1152/jn.00220.2021

9. Sharma P, Naglah A, Aslan S, et al. Preservation of functional descending input to paralyzed upper extremity muscles in motor complete cervical spinal cord injury. *Clin Neurophysiol*. 2023;150:56-68. doi:10.1016/j.clinph.2023.03.003

10. Wahlgren C, Levi R, Amezcua S, Thorell O, Thordstein M. Prevalence of discomplete sensorimotor spinal cord injury as evidenced by neurophysiological methods: A cross-sectional study. *J Rehabil Med*. 2021;53(2):jrm00156. doi:10.2340/16501977-2774

11. Del Vecchio A, Sylos-Labini F, Mondì V, et al. Spinal motoneurons of the human newborn are highly synchronized during leg movements. *Sci Adv*. 2020;6(47). doi:10.1126/sciadv.abc3916

12. Del Vecchio A, Germer CM, Elias LA, et al. The human central nervous system transmits common synaptic inputs to distinct motor neuron pools during non-synergistic digit actions. *J Physiol*. 2019;597(24):5935-5948. doi:10.1113/JP278623

13. Farina D, Holobar A. Characterization of Human Motor Units From Surface EMG Decomposition. *Proc IEEE*. 2016;104(2):353-373. doi:10.1109/JPROC.2015.2498665

14. Mendez Guerra I, Barsakcioglu DY, Vujaklija I, Wetmore DZ, Farina D. Far-field electric potentials provide access to the output from the spinal cord from wrist-mounted sensors. *J Neural Eng*. 2022;19(2). doi:10.1088/1741-2552/ac5f1a

15. Cakici AL, Osswald M, De Oliveira DS, et al. A Generalized Framework for the Study

of Spinal Motor Neurons Controlling the Human Hand During Dynamic Movements. *Proc Annu Int Conf IEEE Eng Med Biol Soc EMBS*. 2022;2022-July:4115-4118. doi:10.1109/EMBC48229.2022.9870914

16. Fuglevand AJ, Lester RA, Johns RK. Distinguishing intrinsic from extrinsic factors underlying firing rate saturation in human motor units. *J Neurophysiol*. 2015;113(5):1310-1322. doi:10.1152/jn.00777.2014

17. Enoka RM. Physiological validation of the decomposition of surface EMG signals. *J Electromyogr Kinesiol*. 2019;46(February):70-83. doi:10.1016/j.jelekin.2019.03.010

18. Heckman CJ, Enoka RM. Motor unit. *Compr Physiol*. 2012;2(4):2629-2682. doi:10.1002/cphy.c100087

19. Holobar A, Minetto MA, Farina D. Accurate identification of motor unit discharge patterns from high-density surface EMG and validation with a novel signal-based performance metric. *J Neural Eng*. 2014;11(1). doi:10.1088/1741-2560/11/1/016008

20. Del Vecchio A, Holobar A, Falla D, Felici F, Enoka RM, Farina D. Tutorial: Analysis of motor unit discharge characteristics from high-density surface EMG signals. *J Electromyogr Kinesiol*. 2020;53:102426. doi:10.1016/j.jelekin.2020.102426

21. Oliveira DS de, Casolo A, Balshaw TG, et al. Neural decoding from surface high-density EMG signals: influence of anatomy and synchronization on the number of identified motor units. *J Neural Eng*. 2022;19(4):046029. doi:10.1088/1741-2552/ac823d

22. Moritz CT, Barry BK, Pascoe MA, Enoka RM. Discharge rate variability influences the variation in force fluctuations across the working range of a hand muscle. *J Neurophysiol*. 2005;93(5):2449-2459. doi:10.1152/jn.01122.2004

23. Proudfoot M, van Ede F, Quinn A, et al. Impaired corticomuscular and interhemispheric cortical beta oscillation coupling in amyotrophic lateral sclerosis. *Clin Neurophysiol*. 2018;129(7):1479-1489. doi:10.1016/j.clinph.2018.03.019

24. Fisher KM, Zaaimi B, Williams TL, Baker SN, Baker MR. Beta-band intermuscular coherence: A novel biomarker of upper motor neuron dysfunction in motor neuron disease. *Brain*. 2012;135(9):2849-2864. doi:10.1093/brain/aws150

25. Norton JA, Gorassini MA. Changes in cortically related intermuscular coherence accompanying improvements in locomotor skills in incomplete spinal cord injury. *J*

Neurophysiol. 2006;95(4):2580-2589. doi:10.1152/jn.01289.2005

26. Nishimura Y, Morichika Y, Isa T. A subcortical oscillatory network contributes to recovery of hand dexterity after spinal cord injury. *Brain*. 2009;132(3):709-721. doi:10.1093/brain/awn338

27. Bräcklein M, Barsakcioglu DY, Vecchio A Del, Ibáñez J, Farina D. Reading and Modulating Cortical b Bursts from Motor Unit Spiking Activity. *J Neurosci*. 2022;42(17):3611-3621. doi:10.1523/JNEUROSCI.1885-21.2022

28. Raptis H, Burtet L, Forget R, Feldman AG. Control of wrist position and muscle relaxation by shifting spatial frames of reference for motoneuronal recruitment: Possible involvement of corticospinal pathways. *J Physiol*. 2010;588(9):1551-1570. doi:10.1113/jphysiol.2009.186858

29. Long J, Federico P, Perez MA. A novel cortical target to enhance hand motor output in humans with spinal cord injury. *Brain*. 2017;140(6):1619-1632. doi:10.1093/brain/awx102

30. Baker SN, Perez MA. Reticulospinal contributions to gross hand function after human spinal cord injury. *J Neurosci*. 2017;37(40):9778-9784. doi:10.1523/JNEUROSCI.3368-16.2017

31. Baker SN. The primate reticulospinal tract, hand function and functional recovery. *J Physiol*. 2011;589(23):5603-5612. doi:10.1113/jphysiol.2011.215160

32. Barsakcioglu DY, Bracklein M, Holobar A, Farina D. Control of Spinal Motoneurons by Feedback from a Non-Invasive Real-Time Interface. *IEEE Trans Biomed Eng*. 2021;68(3):926-935. doi:10.1109/TBME.2020.3001942

33. Simon AM, Hargrove LJ, Lock BA, Kuiken TA. Target Achievement Control Test: Evaluating real-time myoelectric pattern-recognition control of multifunctional upper-limb prostheses. *J Rehabil Res Dev*. 2011;48(6):619. doi:10.1682/JRRD.2010.08.0149

34. Nowak M, Vujaklija I, Sturma A, Castellini C, Farina D. Simultaneous and Proportional Real-Time Myocontrol of Up to Three Degrees of Freedom of the Wrist and Hand. *IEEE Trans Biomed Eng*. 2023;70(2):459-469. doi:10.1109/TBME.2022.3194104

35. Bockbrader M, Annetta N, Friedenberg D, et al. Clinically Significant Gains in Skillful Grasp Coordination by an Individual With Tetraplegia Using an Implanted Brain-

Computer Interface With Forearm Transcutaneous Muscle Stimulation. *Arch Phys Med Rehabil*. 2019;100(7):1201-1217. doi:10.1016/j.apmr.2018.07.445

36. Simeral JD, Kim SP, Black MJ, Donoghue JP, Hochberg LR. Neural control of cursor trajectory and click by a human with tetraplegia 1000 days after implant of an intracortical microelectrode array. *J Neural Eng*. 2011;8(2). doi:10.1088/1741-2560/8/2/025027

37. Wandelt SK, Kellis S, Bjånes DA, et al. Decoding grasp and speech signals from the cortical grasp circuit in a tetraplegic human. *Neuron*. 2022;110(11):1777-1787.e3. doi:10.1016/j.neuron.2022.03.009

38. Blabe CH, Gilja V, Chestek CA, Shenoy K V., Anderson KD, Henderson JM. Assessment of brain-machine interfaces from the perspective of people with paralysis. *J Neural Eng*. 2015;12(4). doi:10.1088/1741-2560/12/4/043002

39. Lahr J, Schwartz C, Heimbach B, Aertsen A, Rickert J, Ball T. Invasive brain-machine interfaces: A survey of paralyzed 'patients' attitudes, knowledge and methods of information retrieval. *J Neural Eng*. 2015;12(4). doi:10.1088/1741-2560/12/4/043001

40. Sierotowicz M, Scheidl MA, Castellini C. Adaptive Filter for Biosignal-Driven Force Controls Preserves Predictive Powers of sEMG. *Proceedings of ICORR 2023*. IEEE 2023. doi: 10.1109/ICORR58425.2023.10304772

Figure legends

Figure 1 Overview of experimental setup and motor unit data analysis (**A**) Experimental setup consisting of 320 surface EMG electrodes placed in the forearm muscles. The movement instructions were guided by a virtual hand video displayed on a monitor in front of the subject. (**B**) A few example electrodes show raw HDsEMG signals while the subject attempts a grasp task (flexion and extension of the fingers, 0.5Hz). (**C**) Example of spatial mapping based on the root mean square values of the motor unit action potential. (**D**) Raster plot of motor unit firings (color-coded) identified during 10s of a grasp task. (**E**) Neural modules extracted for the same task, using factorization analysis. (**F**) Pearson correlation values (r) of the individual motor units with the two neural modules. (**G**) Neural modules' power spectra, showing a peak at the movement frequency (0.5Hz). (**H**) Coherence between cumulative spike trains of motor units across all tasks of subject 6 (S6), highlighting alpha

and beta bands. (**I**) Coherence peak across all tasks of S6 for delta (1-5Hz), alpha (6-12Hz), beta (15-30Hz), and gamma (31-80Hz) bandwidths. The dashed line in red in (H) and (I) indicates the coherence threshold (average coherence between 100-250Hz).

Figure 2 Number of detected motor units and residual HDsEMG signals. (**A**) Example of raw HDsEMG signals for both groups, SCI (pink) and control (blue). The signals are shown in time windows of 20s and 1s. (**B**) Number of detected motor units across subjects for both groups, SCI and control (the dots are color-coded for the subjects of the SCI group). (**C**) Number of detected motor units across all tasks (the dots represent the tasks). (**D**) Distribution of the total number of motor units across groups, SCI in pink and control in blue. (**E**) Example of EMG channels from both SCI and control groups overlayed with the reconstructed EMG. (**F**) Root mean square error (RMSE) between EMG and reconstructed EMG, representing the residual EMG activity for both groups. ***p-value < 0.001.

Figure 3 Discharge rate. (**A)** Average discharge rate across subjects for both groups (the dots are color-coded for the subjects of the SCI group). (**B**) Average discharge rate across all tasks (the dots represent the tasks). (**C**) Distribution of the total number of motor units across groups, SCI in pink and control in blue.

Figure 4 Coherence. (**A**) Average coherence across all participants and all tasks for both groups, SCI in pink and control in blue. The black dashed line represents the coherence threshold (average coherence between 100-250Hz). Each curve in grey represents the coherence for one subject. (**B**-**E**) Area under coherence curve across all subjects and groups for delta (1-5Hz), alpha (6-12Hz), beta (15-30Hz), and gamma (31-80Hz) bands, respectively (the dots represent the tasks and are color-coded for the subjects of the SCI group). For each frequency band, we also show the group distribution of the coherence area values across all tasks and subjects. *0.01 < p-value < 0.05; **0.001 < p-value < 0.01.

Figure 5 Real-time control of motor units and virtual hand. (**A**) Raster plot for all motor units identified for S6 during the respective task (color-coded) and the virtual hand movement trajectories (grey line). Note the task-modulated activity of the motor unit firing

patterns that encoded flexion and extension movements. (**B**) Real-time tasks for two participants (S1 and S6). (**C**) The participants were asked to follow a trajectory on a screen (green line) by attempting a grasp movement. The motor units were decomposed online, and the cumulative smoothed discharge rate (yellow line) was used as biofeedback. After a few seconds of training (**D**), the subjects could track the trajectories with high accuracy and at different target levels (C). (**E**) Cross-correlation coefficient (R) between the smoothed discharge rate and the requested tasks for 4 subjects. (**F**) After the online motor unit decomposition, we used a supervised machine learning method to proportionally control the movement of a virtual hand. Four out of six subjects were able to proportionally open and close the hand (**G-I),** and proportionally control in both movement directions (flexion and extension) the index finger (**H-I**). These subjects were able to control four degrees of freedom (DoFs) that corresponded to hand opening, closing, index flexion, and extension. These subjects were able to control four degrees of freedom (DoFs) that corresponded to hand opening, closing, index flexion, and extension.

Figure 6 Examples of raw HDsEMG signals and spatial amplitude maps. We report examples of EMG signals for all subjects of the SCI group (S1-S8) during index and grasp tasks. The normalized signals from the three EMG channels with higher root mean square (RMS) values (in black) are presented during 5s, together with the virtual hand kinematics (in grey). For each subject, we show a spatial map based on the RMS values of each EMG channel. For brevity, we only present data from eight control group participants for comparison.

Table 1 Characteristics of research participants

Subject	Age (years)	Gender	Injury level	AIS	Wrist movement	Time since injury (years)	Sensory level[a]	Spasticity upper limb (MAS)[b]	Note	Stretch reflexes upper limb	MUs/task[c]	Unique MUs/task[c]
S1	39	Male	C6	B	Yes	18.8	S5	0	Tenodesis	Absent	14.5 ± 2	10.1 ± 2.3
S2	34	Male	C5	B	Yes	9.1	C5	0	Tenodesis	B: reduced; BR, T: absent	8.1 ± 1.2	5.7 ± 1.7
S3	41	Female	C6	B	Yes	24.2	C6	0	Tenodesis	B, BR: exaggerated; T: absent	3.5 ± 1.4	0.8 ± 1.6
S4	39	Female	C5	A	Yes	24.2	C5	0	-	Normal	7.3 ± 2.3	3.7 ± 1.3
S5	34	Male	C6	A	No	22.2	C6	0	-	Absent	8.4 ± 0.7	8.3 ± 0.7
S6	57	Male	C5	A	No	6.9	T3	Right: 2, left: 0	Botox right arm	Right: reduced; left: exaggerated	22.8 ± 4.2	21.1 ± 3.2
S7	44	Male	C6	C	No	18.2	C6	Right: 2, left: 0	-	Right: exaggerated; left: reduced	7.4 ± 2	4.4 ± 2.7
S8	38	Female	C5	B	Yes	5.0	T1	1	-	Absent	5.9 ± 1.2	4.8 ± 1.6

AIS = ASIA Impairment Scale; B = Biceps reflex; BR = Brachioradialis reflex; MAS = Modified Ashworth Scale; T = Triceps reflex.
[a]The sensory level corresponds to lowest level with normal sensory function.
[b]Spasticity was assessed for elbow flexion.
[c]Average number of motor units (MUs) identified per task (mean ± SD) for each subject

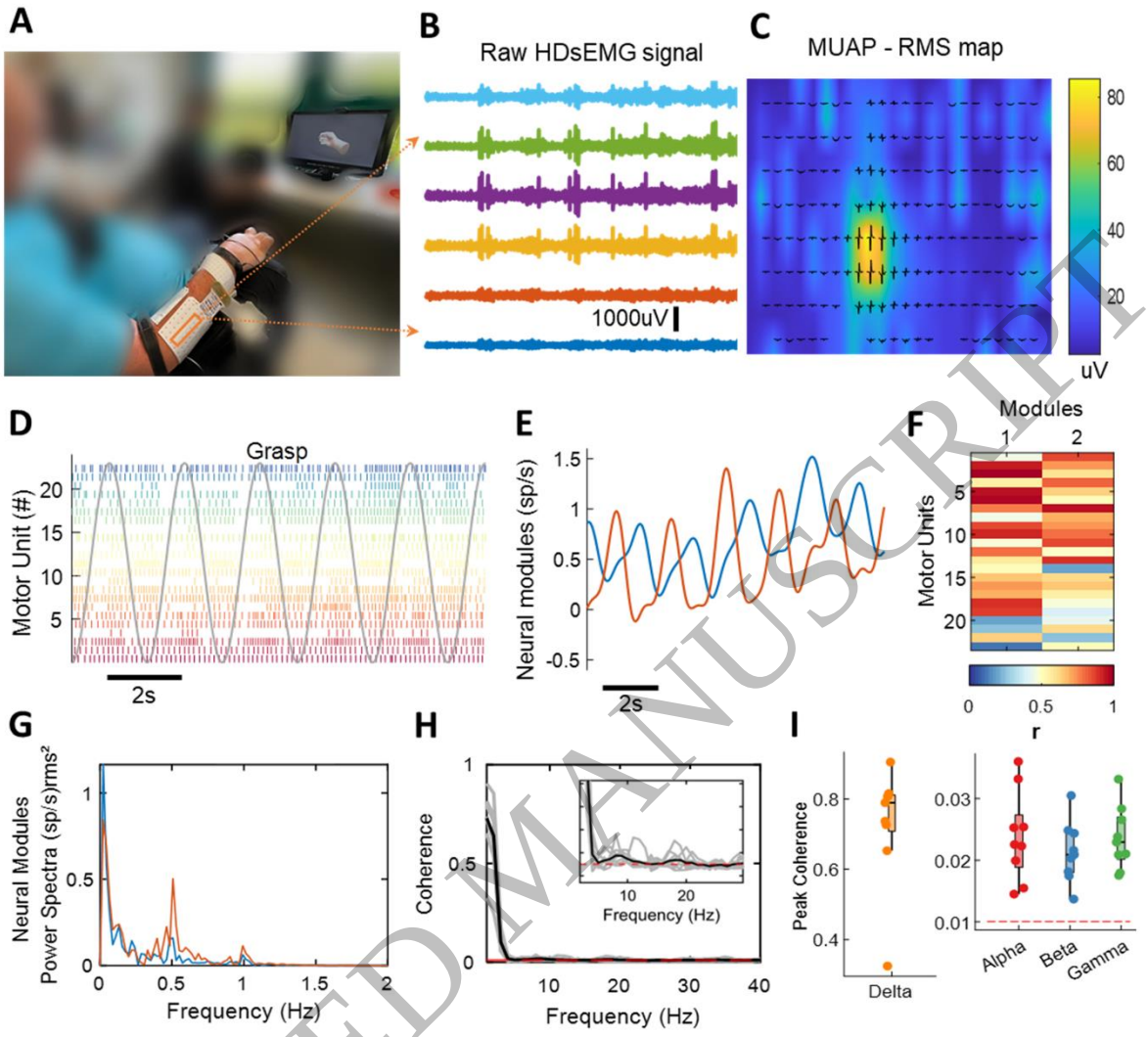

Figure 1
190x172 mm (x DPI)

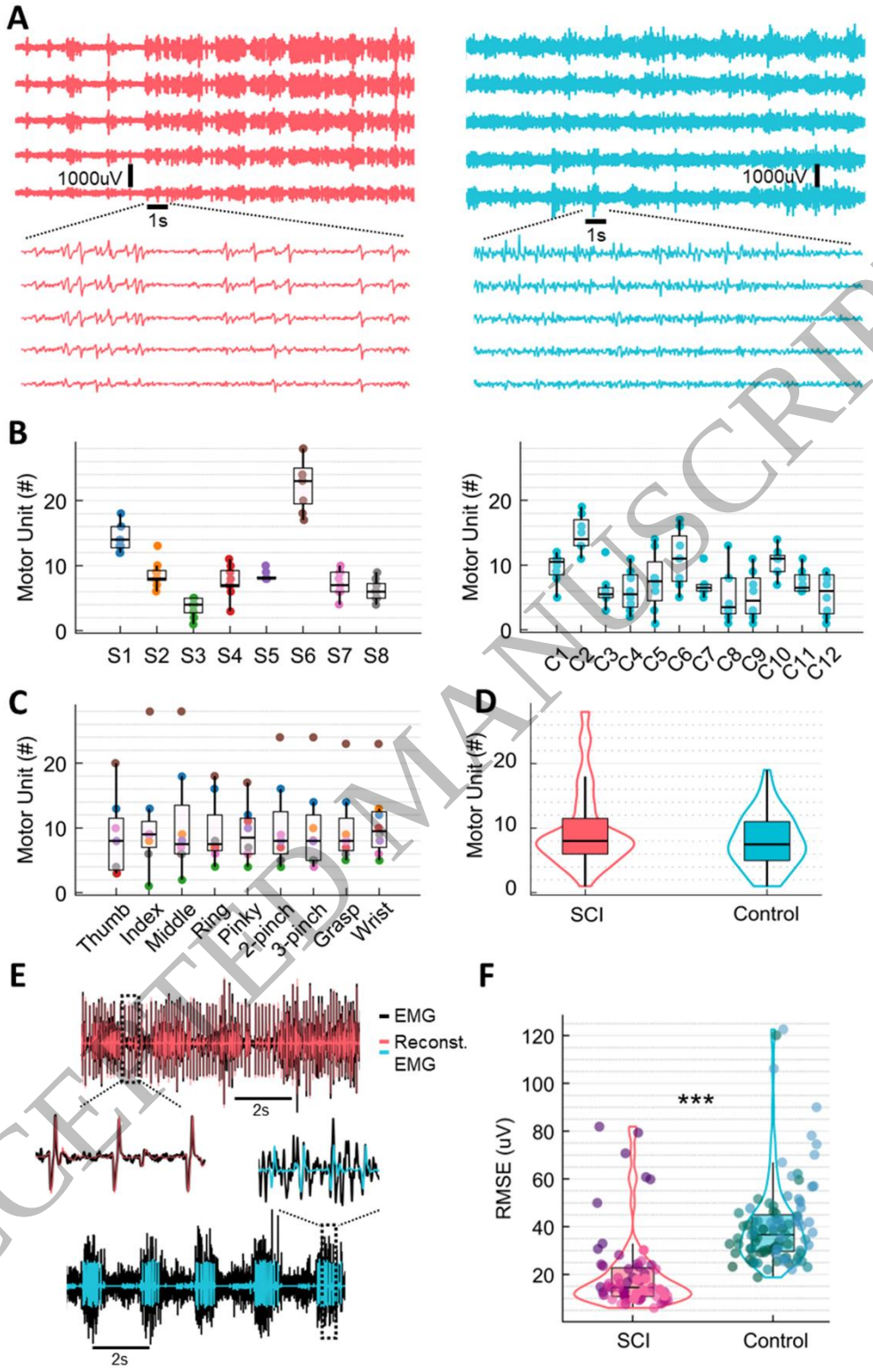

Figure 2
158x243 mm (x DPI)

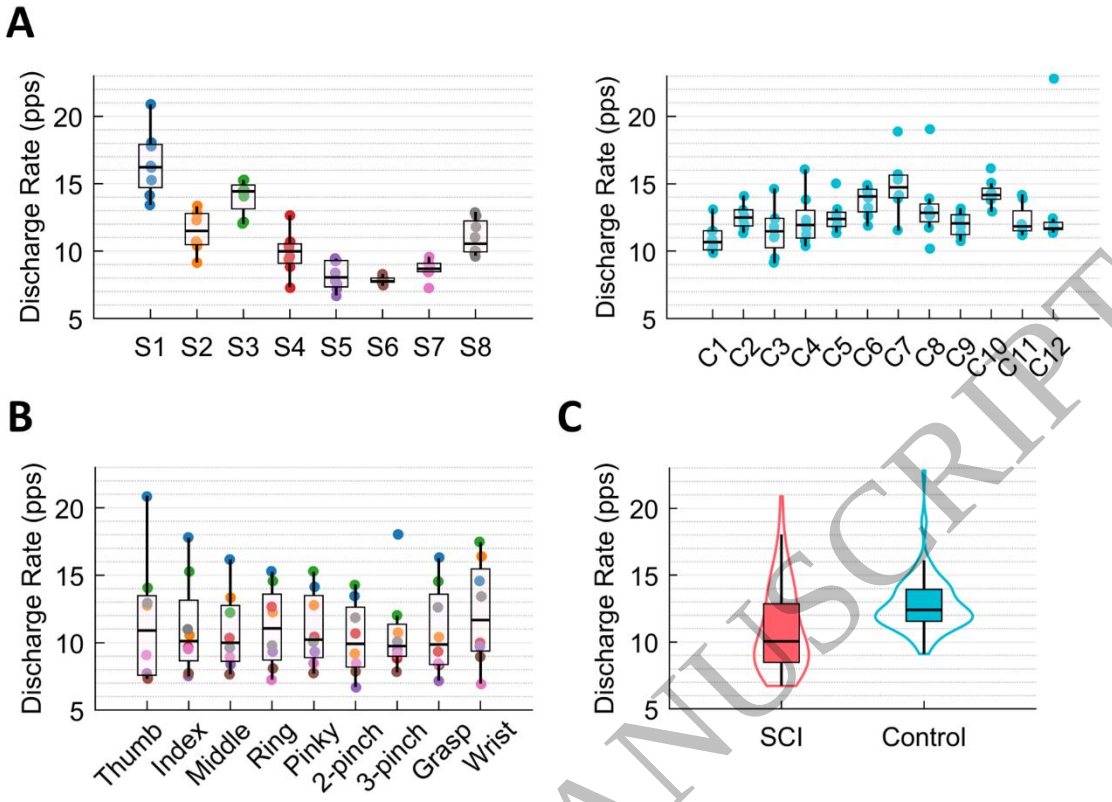

Figure 3
149x109 mm (x DPI)

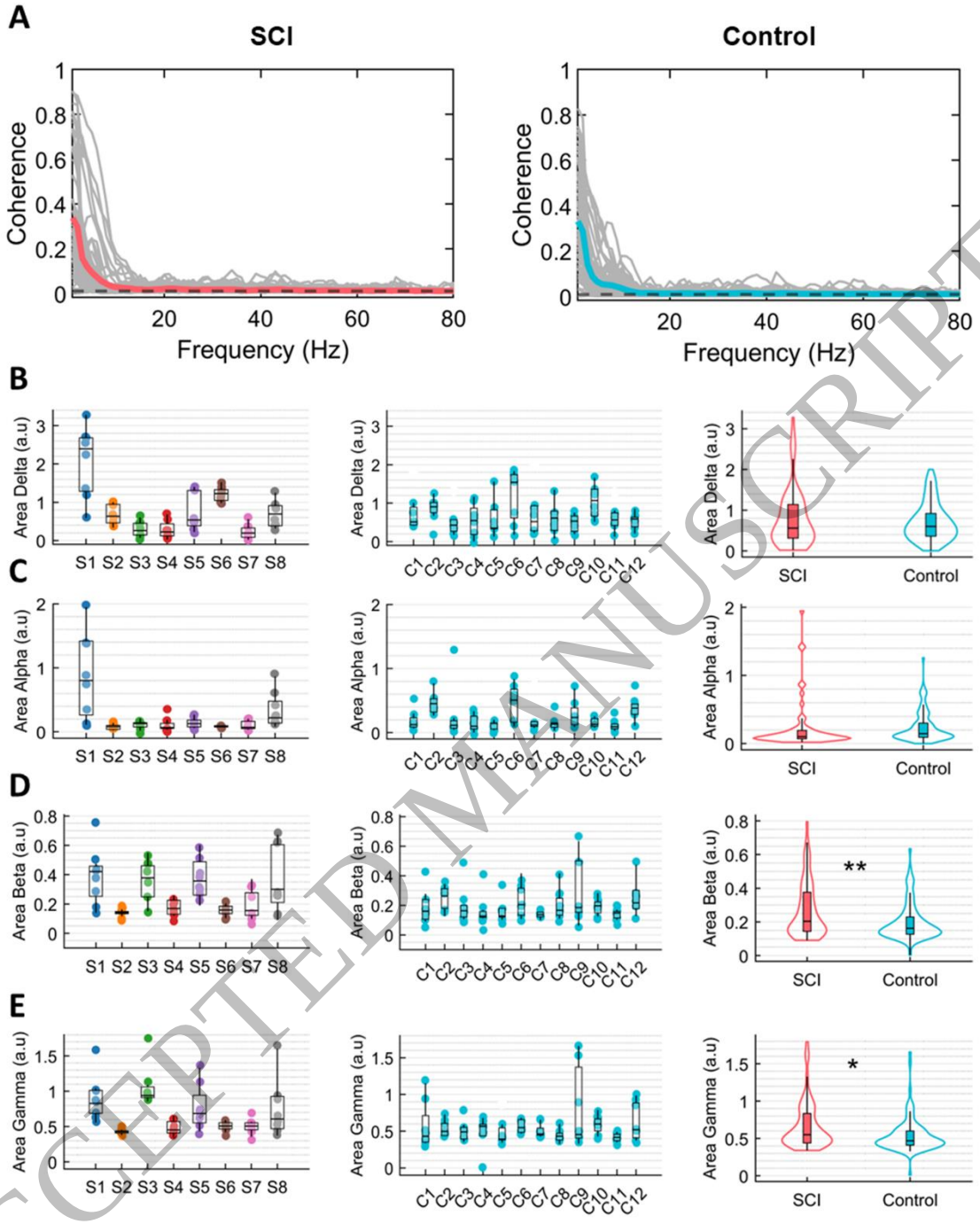

Figure 4
190x220 mm (x DPI)

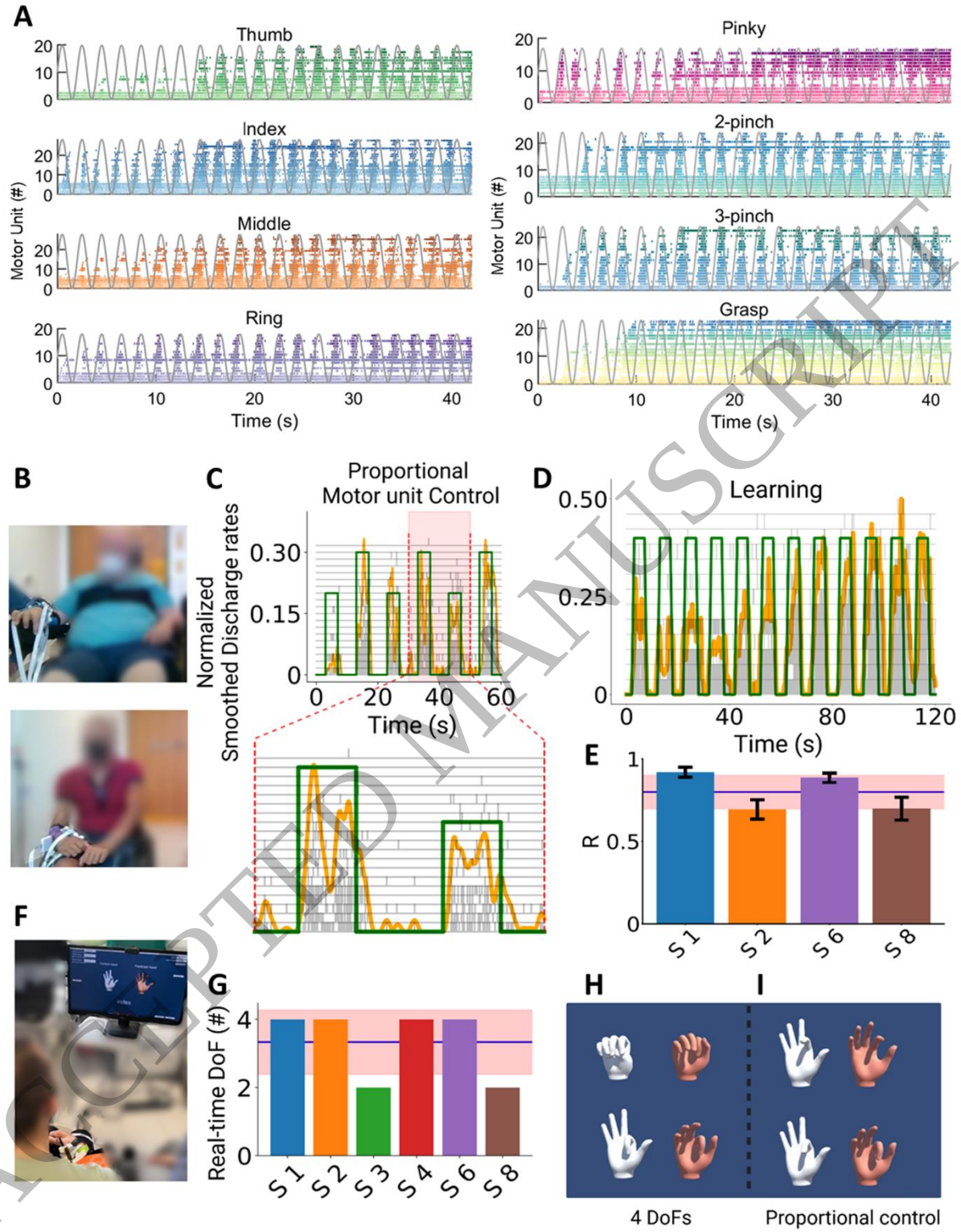

Figure 5
190x246 mm (x DPI)

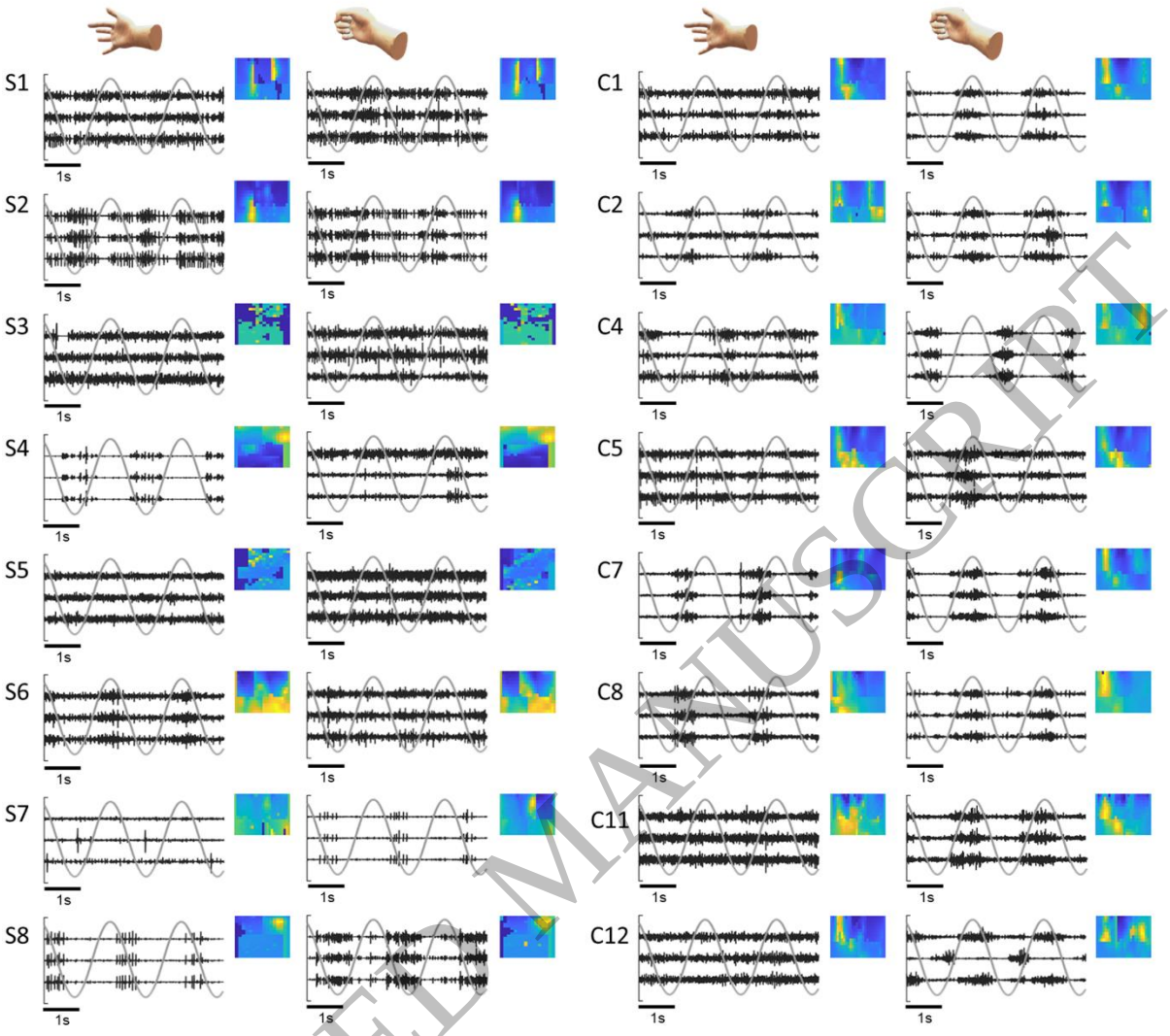

Figure 6
190x172 mm (x DPI)